Magazine of Concrete Research, 1994, **46**, No. 166, Mar., 39–48

A plasticity analysis of anchorage zones

T. J. Ibell* and C. J. Burgoyne*

CAMBRIDGE UNIVERSITY

This Paper is the second of three on the behaviour of anchorage zones for prestressed concrete. Details are presented of a plasticity approach to the ultimate strength analysis of concrete prisms strip-loaded through rigid steel plates. Such a loading arrangement is assumed to represent adequately the transfer of force from tendon to concrete at the anchorage of a prestressed concrete structure. The effects of steel reinforcement are included in the analysis, which is assumed to satisfy plane strain conditions. The Modified Mohr-Coulomb failure criterion with non-zero tension cut-off is used for the concrete. A model, based on experimental evidence, is used as the basis for the plastic analysis, and good correlation is obtained between the theory developed here and the observed test results. It is concluded that such a plasticity approach is useful in assessing the strength of concrete under concentrated load.

Notation

a	half-breadth of test specimens
a_1	half-length of loading plate
c_c	cohesion of the concrete
f_c	'effective' concrete compressive strength
f_{cu}	concrete cube compressive strength
f_t	'effective' concrete tensile strength
f_t'	concrete split-tensile strength
h	height of concrete prism
l_c	length of basal crushing extent
l^{yl}	full length of wedge yield line
l_i^{yl}	length of section i of wedge yield line
r_i	lever arm from point O to any point i on wedge
r_{si}	lever arm from point O to steel crossing point i on wedge
r^R	lever arm from centre of relative rotation to any point on wedge
u	resultant relative displacement between two rigid blocks
u_1, u_2	vertical and horizontal (respectively) components of u
w	width of test specimens
x, y, x	axis labels
x_o, y_o	x and y co-ordinates of the inner limit of basal crushing
x_R, y_R	x and y co-ordinates of the centre of relative rotation
z_i	angle between r_i and the vertical
z_{si}	angle between r_{si} and the vertical
A_s	total area of reinforcing steel crossing a plane
C	basal frictional force
D	total energy dissipated along a yield line by concrete shearing
$\dot{D}$	energy dissipation rate along a yield line by concrete shearing
F_o	compressive force acting on half-wedge
P	applied ultimate load capacity
P^*	predicted ultimate load capacity
P_{init}	initial estimated load capacity of prism
T	total tensile force exerted by the steel reinforcement
W_{base}	basal work done by concrete crushing
W_{system}	total energy dissipated by the entire system
$W_{concrete}$	energy dissipated by concrete shearing
W_E	total external work done on the system
α	angle between yield line and relative displacement vector
α_i	angle between yield line and relative displacement vector at point i
α_{si}	angle between yield line and relative displacement vector at steel crossing point i
β	half-wedge failure angle (to the vertical)
γ_{nt}	shear strain across a yield line
δ	relative displacement vector between two rigid blocks
δ_i	relative displacement vector between two rigid blocks at point i
δ_{si}	relative displacement vector between two rigid blocks at steel crossing point i
δ_n, δ_t	normal and tangential components of δ
Δ	width of yield line
ϵ_1, ϵ_2, ϵ_3	principal strains

* University of Cambridge, Engineering Department, Trumpington St., Cambridge, CB2 1PZ, UK.
Paper received 29 June 1993.

ϵ_n normal strain across a yield line
ϵ_t tangential strain across a yield line
η relative rotation of rigid blocks across a yield line
θ angle between r^R and the horizontal
κ angle between yield line and horizontal
ν 'effectiveness factor' for concrete
ν_t 'tensile effectiveness factor' for concrete
ϕ internal angle of friction of concrete
σ_1, σ_2, σ_3 principal stresses

Introduction

In a previous Paper[1], failure mechanisms of centrally strip-loaded concrete prisms were reported in some detail. It was found that, in general, failure of these strip-loaded prisms occurred in a two-step process. Initial central cracking, extending nearly the full length of the specimens, preceded planar wedge formation beneath the loading plate. Figure 1 shows the overall loading arrangement, steel reinforcement layout and general wedging failure mechanism of the test specimens of Ref. 1. The present problem may thus be considered as a case of shearing along yield lines at failure, which has been studied extensively by several researchers,[2–6] with some favourable correlations between such plasticity methods and test results being obtained. It was thus considered worthwhile to apply the upper- and lower-bound methods of analysis to the present problem.

Preliminary assumptions

The following assumptions are made regarding the plasticity solutions formulated in this Paper.

(*a*) Rigid perfectly-plastic collapse occurs. Elastic deformations are negligible.
(*b*) The Modified Mohr-Coulomb failure criterion with non-zero tension cut-off is assumed for the concrete in areas of shear-tension or shear-compression failure. Figure 2 shows details of this failure surface. The internal angle of friction, ϕ, is assumed to be a constant 37°[3,6] for all combinations of stress. In separation failures, a limiting tensile strength of concrete is assumed, where applicable.
(*c*) The steel bars carry axial tension forces only. Any dowel effects are ignored.

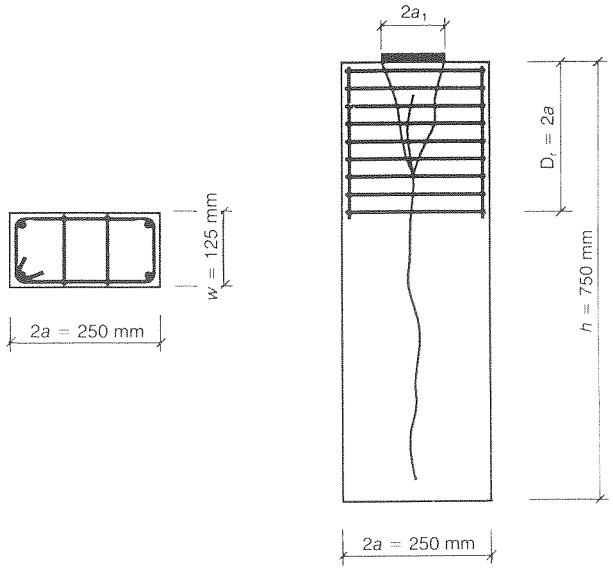

Fig. 1. Overall arrangement of the test specimens, showing typical steel reinforcement and final wedging failure

The 'effective' strength of concrete

It is not possible in practice for a reinforced concrete structure to undergo large deformations at a constant stress level, which is a necessary assumption in a rigid-plastic collapse idealisation.[3] Moreover, the stress–strain curve

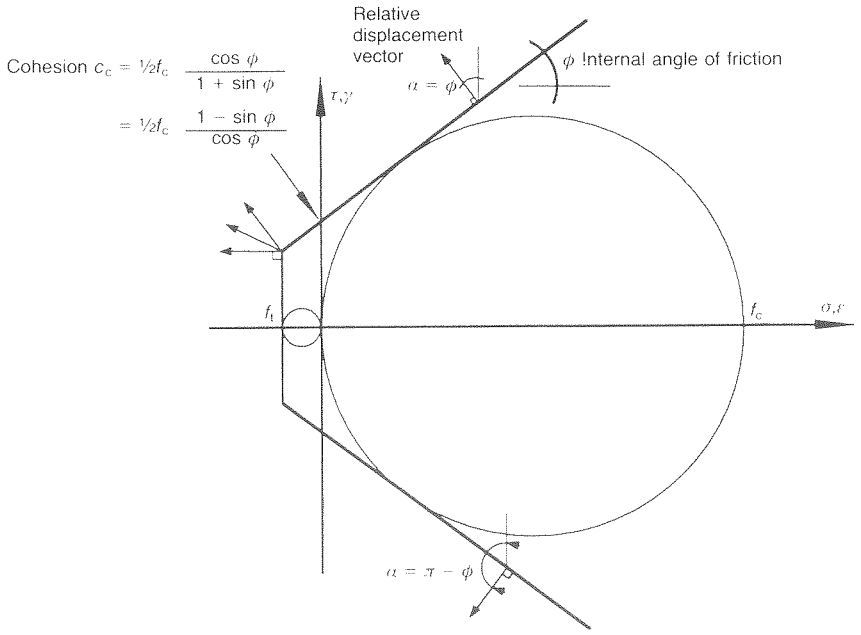

Fig. 2. The Modified Mohr-Coulomb failure criterion, with non-zero tension cut-off

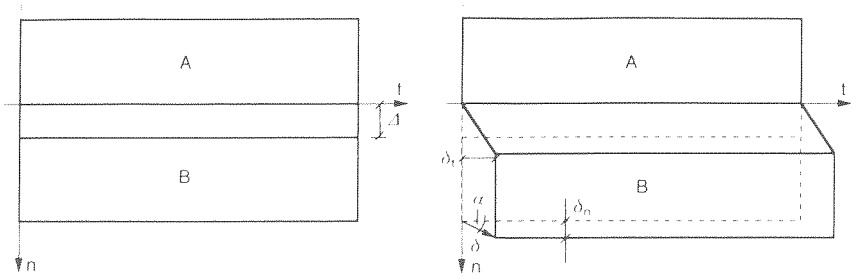

Fig. 3. Discontinuity zone between two rigid blocks under relative displacement

for concrete in compression has a falling branch beyond its ultimate strength, and ductility is limited. Therefore, in order to obtain reasonably satisfactory predictions using the assumptions of rigid-plastic collapse, a reduced strength of concrete must be assumed. The 'effectiveness factor', ν, is introduced to create an effective concrete strength, f_c, which is equal to νf_{cu}, f_{cu} being the measured compressive cube strength of the concrete. Similarly, the 'tensile effectiveness factor', ν_t, is used to reduce the tensile strength of the concrete, f_t', to f_t, for similar reasons. Several values of ν are assumed for a variety of problems, but for the case of shearing in concrete, $\nu = 0{\cdot}67$ has been suggested[5,7] and is assumed throughout this Paper. A range of effective tensile strengths of concrete has also been suggested by Chen and Drucker,[2] varying from as high as $f_t = f_c/5$ to $f_t = 0$, for purposes of comparison with specific test results.

Upper-bound analysis

Formulation of planar rigid-plastic upper-bound methods

The following formulation is documented in Nielsen's book,[3] but is included here for completeness. Consider two rigid blocks, A and B, separated by a distance Δ, as shown in Fig. 3. The relative normal and tangential displacements are δ_n and δ_t respectively. The resultant relative displacement is δ, inclined at angle α to the yield line; δ and α are permitted to vary along the full length of the yield line, subject to compatibility requirements.

Consider the thin layer between the rigid blocks. Plastic flow is assumed to occur only in this region. Hence, the plastic strains are

$$\epsilon_t = 0,\ \epsilon_n = \frac{\delta_n}{\Delta},\ \gamma_{nt} = \frac{\delta_t}{\Delta} \tag{1}$$

and

$$\delta_n = \delta \sin \alpha,\ \delta_t = \delta \cos \alpha \tag{2}$$

so that

$$\epsilon_t = 0,\ \epsilon_n = \frac{\delta \sin \alpha}{\Delta},\ \gamma_{nt} = \frac{\delta \cos \alpha}{\Delta} \tag{3}$$

The principal strains are easily shown to be

$$\epsilon_1 = \frac{1}{2}\frac{\delta}{\Delta}(\sin \alpha + 1) \tag{4a}$$

$$\epsilon_2 = \frac{1}{2}\frac{\delta}{\Delta}(\sin \alpha - 1) \tag{4b}$$

The energy dissipation rate per unit length of yield line, for an element of unit thickness, is

$$\dot{D} = \Delta(\sigma_1\epsilon_1 + \sigma_2\epsilon_2) \tag{5}$$

where σ_1 and σ_2 are the principal stresses corresponding to the principal strains ϵ_1 and ϵ_2.

By combining the above equations, it can be shown that for a plane stress problem, assuming the tensile strength of concrete is negligible,

$$\dot{D} = \frac{1}{2}f_c\delta(1 - \sin \alpha) \text{ per unit length} \tag{6}$$

in the full range $0 \leq \alpha \leq 2\pi$.

For a plane strain problem, once again ignoring the tensile strength of concrete, equation (6) still holds, but a restriction is placed on α such that $\phi \leq \alpha \leq \pi - \phi$, where ϕ is the internal angle of friction for concrete. (See Fig. 2).

Uniform translation of outer blocks at failure

Chen and Drucker[2] carried out a plane strain analysis of an unreinforced concrete prism strip-loaded as shown in Fig. 4. Planar failure of this type was encountered in virtually all of the present tests.[1] This mode is assumed throughout the present analysis, even though Chen and Drucker postulated that such behaviour ought only to occur for $h < 2a$. (For $h > 2a$, the mechanism of failure proposed by Chen and Drucker contained no longitudinal central crack, but rather inclined slip planes beneath the wedging region.) They assumed that the two outer surrounding blocks (II) in Fig. 4 translate laterally on a frictionless base during wedging failure.

Using the velocity relations from Fig. 4, and applying equation (6), together with a term for the inclusion of separation work along the central crack (under the assumption that such work can indeed exist at collapse), they found the total dissipation, D, to be

$$D = \left(\frac{1 - \sin \phi}{2}\right)f_c\frac{2a_1w}{\sin \beta}u + 2wf_t(h - a_1 \cot \beta)u \sin(\beta + \phi) \tag{7}$$

where α is here assumed to equal ϕ at failure. The external work, W_E, is given by

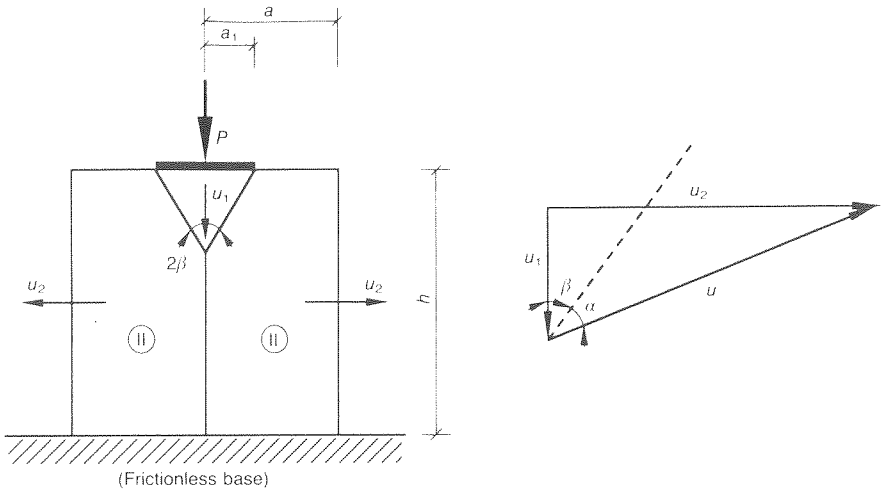

Fig. 4. Chen & Drucker's failure mechanism and velocity relations

$$W_E = P_u \cos(\beta + \phi) \tag{8}$$

Setting these expressions equal, the following upper-bound solution is found.

$$P = \frac{2a_1 w}{\sin\beta \cos(\beta + \phi)} \left[\left(\frac{1 - \sin\phi}{2} \right) f_c + \sin(\beta + \phi) \left(\frac{h}{a_1} \sin\beta - \cos\beta \right) f_t \right] \tag{9}$$

Minimization of (9) with respect to β, and setting $f_t = 0$, produces the trivial solution

$$P = 2a_1 w f_c \tag{10}$$

with $\beta = \pi/4 - \phi/2$.

With non-zero tension cut-off, in the general case, β may be found from

$$\cot\beta = \tan\phi + \sec\phi \times \left[1 + \frac{h/a_1 \cos\phi}{\frac{f_c}{f_t}\left(\frac{1 - \sin\phi}{2} \right) - \sin\phi} \right]^{1/2} \tag{11}$$

Results from experiments[8] showed it to be unlikely that any work could be dissipated along the central crack during failure of the prisms, as this crack formed well before failure in general. There are also conceptual problems with the idea of plastic work in a brittle tensile failure. The contribution of this work was therefore removed entirely from the formulation of the failure load for all subsequent analyses, by assuming that $f_t = 0$.

Chen and Drucker's analysis is extended to include steel reinforcement by neglecting any dowel action, and assuming that stretching of the steel is its only form of energy dissipation. It is also assumed that the steel stirrups are fully yielded at failure, in accordance with experimental observation and plasticity theory alike.

Equation (9) then becomes

$$P = \frac{2a_1 w}{\sin\beta \cos(\beta + \phi)} \left(\frac{1 - \sin\phi}{2} \right) f_c + 2T \tan(\beta + \phi) \tag{12}$$

where T is the total steel force in the yielded bars.

Setting $\partial P/\partial\beta = 0$ for minimum P, it is found that

$$f_c \left(\frac{1 - \sin\phi}{2} \right) \cos(2\beta + \phi) - \frac{2T \sin^2\beta}{2a_1 w} = 0 \tag{13}$$

The non-linear nature of this equation leads to the necessity for a numerical method of solution for β. The Newton-Raphson method was chosen for this purpose. Figure 5 shows detailed comparisons between the above prediction for failure loads and strip-loaded test specimen results. There is reasonable correlation between predictions and experimental results.

The effect of variable positioning of steel reinforcement

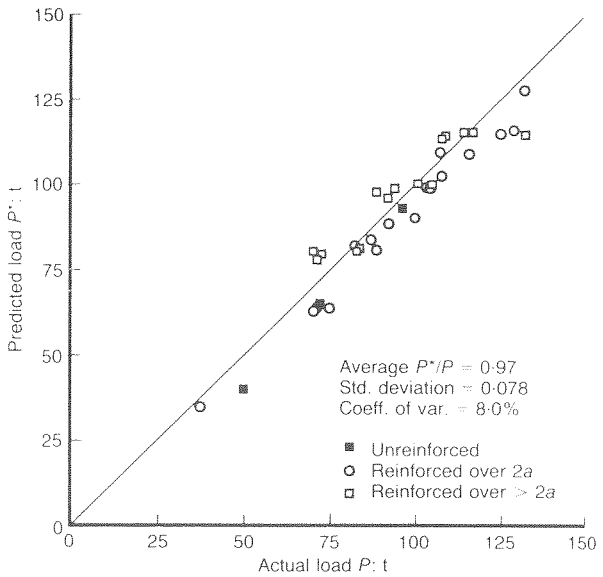

Fig. 5. Comparison between test results and predictions from the translational plasticity model

in the prisms is not modelled by this method, as uniform translation of the blocks is assumed. Note that it is necessary (under the assumption of uniform translation of the outer blocks) to assume that *all* steel has yielded in these specimens, even though it was found experimentally that only steel to a depth of $2 \cdot 4a$ (300 mm) had actually yielded.[9]

Because this method is based on plane strain conditions, the experimental results used for comparison are those in which plane strain conditions were approximated. However, several test specimens failed in an out-of-plane wedging mode[1,8] and such specimens are not included either in Fig. 5 or in the correlation calculations.

Rotation of outer blocks during failure

During failure of the test specimens, it was noticed that the outer blocks rotated outwards about the base, allowing the wedge to penetrate the prism. It was decided to include this rotation of the outer blocks in upper-bound analyses of the problem. Figure 6 shows the general failure mechanism assumed. In the Figure, a straight wedge yield line has been shown, but a curved yield line could also be considered and will be discussed later.

Rotation of the outer blocks is assumed to occur about point O (x_o, y_o) on the base. Point O is the innermost limit of compressive stress on the base, allowing rapid calculation of the resultant reaction force on the base, assuming pure crushing of the basal concrete over this region, with $f_c = 0 \cdot 67 f_{cu}$.

The wedge is assumed to move down by unit displacement. A rotation (η) about point O is chosen and the relative displacement vectors δ_i are found at discrete points p_i along the yield line, as shown in Fig. 7. The angle between the slope of the yield line and the relative displacement vector is α_i.

The energy dissipation rate at point p_i is given by

$$\dot{D}_i = \frac{1}{2} w f_c \delta_i (1 - \sin \alpha_i) \text{ per unit length} \quad (14)$$

from equation (6), for the unreinforced case.

When steel stirrups are present, the extra work dissipated due to stretching of these bars is added to the above expression. In accordance with plasticity theory, it is assumed that *all* steel bars have yielded, even when the steel is spread over depths greater than $2a$, the commonly accepted bursting region in anchorage zone design.[10] Where the steel bars cross the wedge planes (which might be at positions different from those chosen to calculate $\dot{D}_i$ above), the additional energy dissipation, D_{si}, due to this steel alone is

$$D_{si}^{w} = 2A_s^{w} f_y \delta_{si} \sin(\alpha_{si} + \beta) \quad (15)$$

for each double-legged stirrup, where A_s^{w} is the area of a stirrup crossing the wedge plane, and f_y is the yield strength of the steel. Where additional steel bars cross the central crack below the wedge, the extra energy dissipated is

$$D_{si}^{c} = 2A_s^{c} f_y \eta r_{si} \cos z_{si} \quad (16)$$

for each double-legged stirrup, where A_s^{c} is the area of a stirrup crossing the central crack.

In addition to the above work calculations for dissipation along the yield lines, work is also considered to be done on the specimen base, where the concrete crushes. This energy is

$$W_{base} = P_{init} l_c \frac{\eta}{2} \quad (17)$$

where P_{init} is the initially guessed value of failure load and l_c is the length on the base over which crushing is assumed to occur in each outer block.

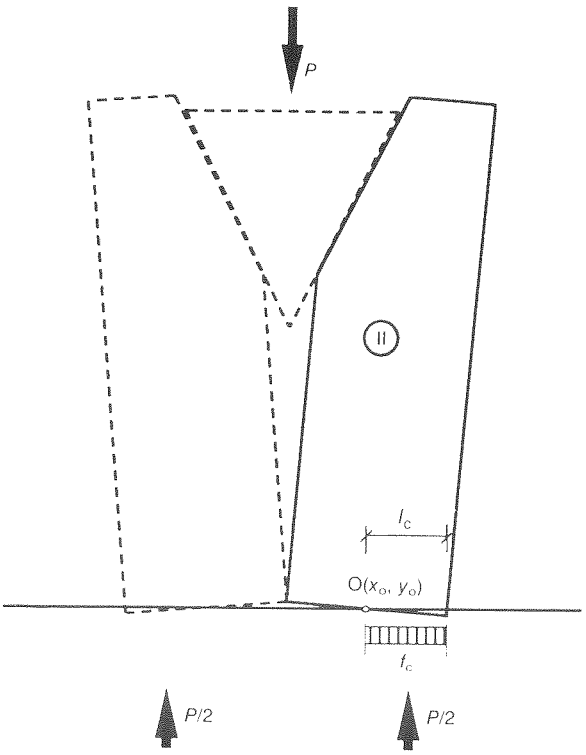

Fig. 6. Rotational model of the experiments, showing position of point O, and equilibrium of forces

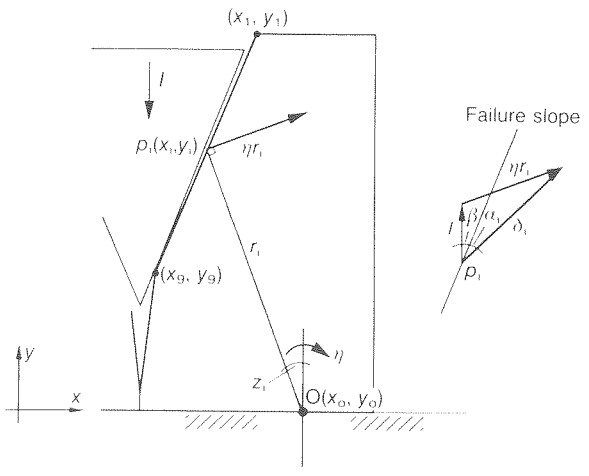

Fig. 7. Failure mechanism and velocity diagram for the rotational plane strain analysis

The total energy dissipation in the system is then found by summing the energy over the length of the yield lines, over the number of stirrups, and over the base, so that

$$W_{\text{system}} = \int_{l^{yl}} \dot{D}_i \, dl + \sum_{i=1}^{NSW} D_{si}^{w} + \sum_{i=NSW+1}^{NS} D_{si}^{c} + W_{\text{base}} \quad (18)$$

where l^{yl} is the total length of both wedge yield lines, NSW is the number of steel stirrups crossing the wedge yield lines and NS is the total number of yielded steel stirrups crossing any yield line in the system.

Two specific formulations are now presented, under differing assumptions.

(*a*) The wedge yield lines are straight, and the bottom point of the yield line has $\alpha = \phi = 37°$, with α increasing in value up the wedge, in accordance with $\phi \leq \alpha \leq \pi - \phi$.
(*b*) The wedge yield lines are curved such that $\alpha_i = \alpha_{si} = \phi = 37°$ at every point along the wedge planes.

Straight wedge yield lines, $\alpha = \phi = 37°$ at bottom of wedge

The detailed steps of this analysis are outlined below.

(*a*) Choose a failure angle, β.
(*b*) Estimate a failure load, P_{init}.
(*c*) Calculate x_o ordinate, based on crushing of basal concrete.
(*d*) Calculate nine sets of co-ordinates, $p_i(x_i, y_i)$, along the yield line, for use in numerical integration.
(*e*) Calculate all co-ordinates, $p_{si}(x_{si}, y_{si})$, of steel stirrups crossing the yield lines (wedge and central crack).
(*f*) Calculate r_i and z_i at each integration point and r_{si} and z_{si} at each steel crossing point.
(*g*) Let the value of α at the bottom of the wedge yield line be ϕ (37°). This defines the rotation η from the velocity relations of Fig. 6.
(*h*) Calculate δ_i and δ_{si} by use of the cosine rule, applied to the velocity relations.
(*i*) Calculate α_i and α_{si}, by use of the sine rule, applied to the velocity relations.
(*j*) Calculate $\dot{D}_i = \left(\frac{1 - \sin \alpha_i}{2}\right) w f_c \delta_i$.
(*k*) Calculate the total energy dissipation in the system, due to concrete shearing, steel stretching, and basal crushing from equation (18), using Simpson's Rule for the numerical integration of the concrete contribution to W_{system}.
(*l*) The guessed external work is $P_{\text{init}} \times 1$ and the corresponding calculated internal work is W_{system}. Therefore, go back to step (*b*), and vary P_{init} until the external and internal work values are close in magnitude. The average value between the computed internal work and the initial estimated external work is used as the updated value of P_{init} for each iteration.
(*m*) Go back to step (*a*) and vary the wedge failure angle, β, until the minimum value of P is found.

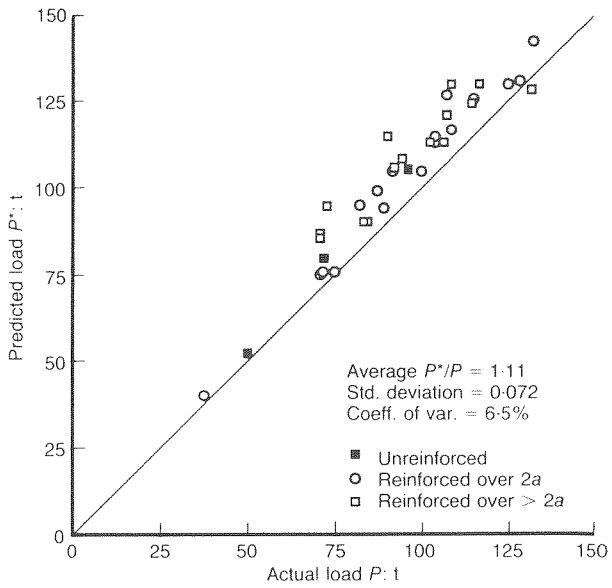

Fig. 8. Comparison between test results and predictions from the rotational plasticity model with $\alpha = \phi = 37°$ at the bottom of the (straight) wedge yield line

In general, between (2) and (10) iterations were necessary to determine the final value of P for each value of β, depending upon the original estimate of P_{init}.

Results from this analysis are shown in Fig. 8 and are compared with the same test results as before. Correlation between theory and experiment is reasonable on the whole, the predictions being about 11% higher than the test results.

The average value of predicted load to actual failure load from Fig. 8 is higher than that of Fig. 5. Thus, the upper-bound method incorporating rotation of the outer blocks predicts higher failure loads than those found under purely translational assumptions. During testing, the rotational mode of failure was indeed observed. The fact that the translational mode is predicted to occur in preference is explained as follows. Frictional forces on the base of the specimens would have attempted to prevent a translational mechanism in the tests. These forces ought thus to be considered in a full translational mechanism model, but have been neglected for simplicity. It does seem, however, that in practice, friction on the base of the specimens allows the rotational mechanism to occur in preference to the translational one.

Curved wedge yield lines, $\alpha = \phi = 37°$ along entire wedge

It was considered possible that the relative displacement angle α could be kept at a constant value of ϕ along the wedge yield line, under rotation of the outer blocks. This implies the formation of a curved yield line to accommodate this behaviour.

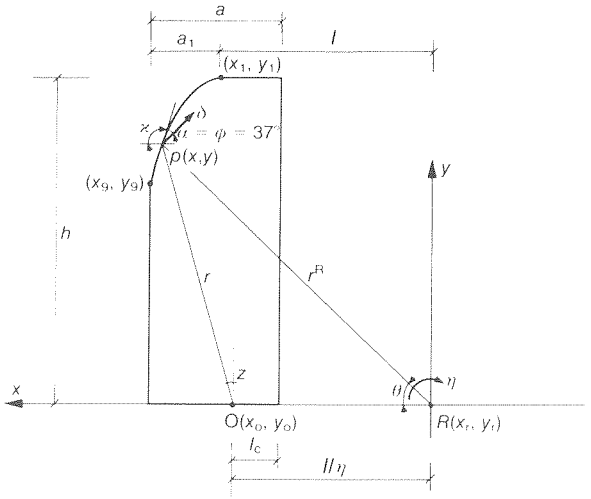

Fig. 9. Rotational model for plane strain analysis, where $\alpha = \phi = 37°$ all along the curved wedge yield line

Consider the curved yield line shown in Fig. 9. Rotation of the outer block occurs about point O. It is assumed that the wedge remains still and the outer block moves vertically up one unit at point O. Combining the rotation and vertical displacement of the outer block, the relative centre of rotation between the wedge and outer block is located at point *R*, a horizontal distance $1/\eta$ from point O.

The value δ is now $\delta = r^R\eta$, (from Fig. 9) and α is the angle between δ and the tangent to the yield line at point $p(x, y)$.

It is desired that $\alpha = \phi = 37°$ everywhere along the wedge. From Fig. 9,

$$\frac{dy}{dx} = \tan(\kappa) \tag{19}$$

or,

$$\frac{dy}{dx} = \tan(\pi - (\pi/2 - \theta) - \phi) \tag{20}$$

$$= \tan(\pi/2 + \theta - \phi) \tag{21}$$

where θ is the angle onto the horizontal from the origin to point p. Also,

$$\theta = \arctan(y/x) \tag{22}$$

so that

$$\frac{dy}{dx} = \tan(\pi/2 + \arctan(y/x) - \phi) \tag{23}$$

The substitution $p = p(x) = y/x$ is made and the differential equation separated into two independent integrals. The solution to this differential equation then takes the form

$$\arctan(y/x) + \cot\phi \ln\left|\frac{1}{\sqrt{(1+(y/x)^2)}}\right| - \cot\phi \ln x + C = 0 \tag{24}$$

where C is a constant of integration which can be found from the known conditions at the top of the prism.

When $y = h$,

$$x = l = 1/\eta - l_c + a - a_1 \tag{25}$$

Whence,

$$C = -\arctan(h/l) - \cot\phi \ln\left|\frac{1}{\sqrt{(1+(h/l)^2)}}\right| + \cot\phi \ln l \tag{26}$$

From equations (24) and (26), the relationship between x and y produces a curved wedge yield line profile.

The detailed steps of the full upper-bound analysis are given below.

(*a*) Estimate a failure load, P_{init}.
(*b*) Choose a rotation, η.
(*c*) Calculate the co-ordinates (x_R, y_R) of point R.
(*d*) Calculate nine (x_i, y_i) co-ordinates along the length of the wedge curve from equations (24) and (26), based on evenly spaced x-ordinates.
(*e*) Calculate all (x_{si}, y_{si}) co-ordinates of steel stirrups crossing the yield lines and central crack.
(*f*) Calculate δ_i and δ_{si} at all relevant points. $\delta_{si} = \eta r_{si}^R$ for all steel stirrups crossing the wedge, and $\delta_{si} = \eta r_{si}$ for all steel stirrups crossing the central crack.
(*g*) Calculate the length (assumed straight) of line l_i^{yl} between each point p_i and p_{i+1} on the yield line.
(*h*) Calculate the energy dissipated in the concrete shearing, per unit length, at each point p_i along the wedge yield line from equation (14), and integrate using Simpson's rule to get $W_{concrete}$.
(*i*) Calculate the total energy dissipation in the system due to concrete shearing, steel stretching and basal crushing.

$$W_{system} = W_{concrete} + \sum_{i=1}^{NSW} A_s^w f_y \delta_{si} \sin\theta_{si} + \sum_{i=NSW+1}^{NS} A_s^c f_y \delta_{si} \cos z_{si} + P_{init} l_c \eta/2$$

(*j*) Go back to step (*b*) and vary η until a minimum value of W_{system} is found.
(*k*) The guessed external work is $P_{init} \times 1$ and the corresponding calculated internal work is W_{system}. Therefore, go back to step (*a*) and estimate a new P_{init}.
(*l*) Repeat until $P_{init} \times 1 = W_{system}$, the minimum internal work for optimum rotation, η.

This method has again been applied to the test specimens of Ref. 4. The results are shown in Fig. 10 together with the test results. The behaviour of the specimens is again predicted reasonably where the assumed mode of failure occurred.

On the whole, this method involving a curved yield line predicts lower failure loads than those from the straight yield line case formulated before, under similar rotational assumptions, but higher failure loads than those under the simple translational assumptions. Therefore, although the rotational mechanisms occurred during testing, the

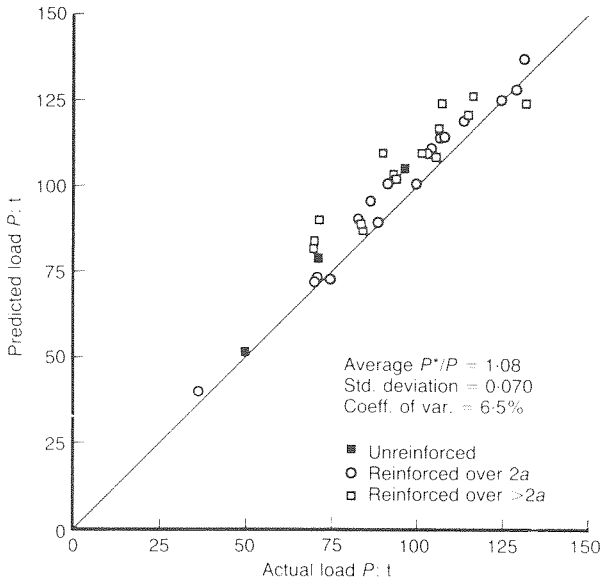

Fig. 10. Comparison between test results and predictions from the rotational plasticity model with $\alpha = \phi = 37°$ all along the length of the (curved) wedge yield line

translational mechanism is again predicted to occur first, due to the neglect of friction on the base of the specimens in this model. If it is therefore considered impossible that such a mechanism can occur in practice, the upper-bound analyses predict a curved yield line to occur in general, with $\alpha = \phi = 37°$ along the length of this yield line. However, the actual failure mechanisms of the test specimens were not studied closely enough for specific geometric comparisons to be made with the theory.

Lower-bound analysis

Equilibrium-based plasticity solution

Consider the failure model of a prism shown in Fig. 11, where the concrete is isolated from the steel. It is assumed in this model that central cracking has occurred along the entire length of the specimen (a similar assumption made under energy-balance calculations before) and that the position of the basal force $P/2$ is central on the half-prism. It is further assumed that an equilibrium force F_0 acts on the half-wedge at the level of the loading plate[11] and that horizontal equilibrium is maintained by a frictional force C on the base of the specimen and the applied steel force T (yielding of all bars occurs). The assumed existence of the frictional force C is based on experimental evidence,[1] where it was found that, in general, before wedging failure, the central crack propagated to within a few centimetres of the base, without actually reaching it.

For overall equilibrium of the half-prism shown, the following conditions must be satisfied.

$$T = C + F_0 \text{ (horiz. equil.)} \qquad (27)$$

and

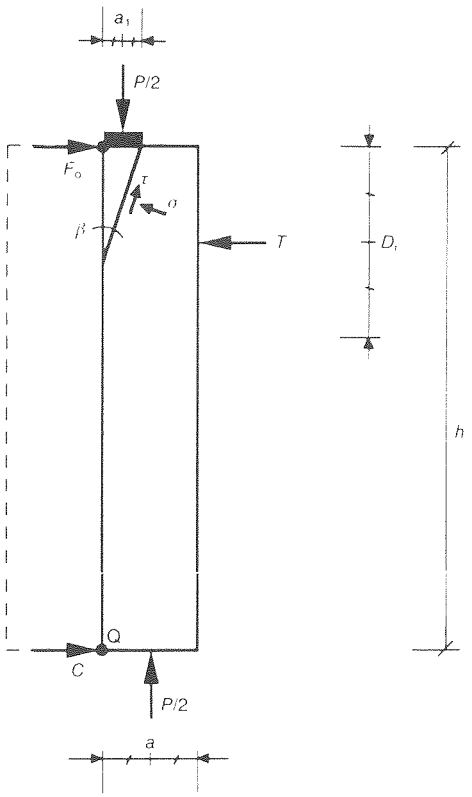

Fig. 11. Lower-bound equilibrium model of failure

$$\frac{P}{2} \cdot \frac{a}{2} + T\left(h - \frac{D_r}{2}\right) = F_0 h + \frac{P}{2} \cdot \frac{a_1}{2}$$

(mom. equil. about Q) (28)

where all symbols are as shown in Fig. 11.

From consideration of the resultant stresses acting on the failure wedge, the following equations of equilibrium may be written, taking σ and τ as uniform along the wedge plane.

$$\tau \frac{a_1 w}{\sin \beta} \cos \beta + \sigma \frac{a_1 w}{\sin \beta} \sin \beta = \frac{P}{2}$$

(vert. equil.) (29)

and

$$\sigma \frac{a_1 w}{\sin \beta} \cos \beta - \tau \frac{a_1 w}{\sin \beta} \sin \beta = F_0$$

(horiz. equil.) (30)

where w is the width of the prism.

In addition, the Modified Mohr-Coulomb failure criterion for concrete states that

$$\tau = c_c + \sigma \tan \phi \qquad (31)$$

along the failure plane.

Equation (31) is substituted into (29) and (30). The expression for F_0 from (28) is then substituted into (30), leaving two simultaneous equations (29) and (30) in unknowns σ and P, under the assumption that the failure wedge half-angle β is a constant.

Solution of these equations yields the expression for a given in equation (32).

$$\sigma = \frac{a_1 whc_c + \frac{1}{2}aa_1 wc_c \cot\beta - \frac{1}{2}a_1^2 wc_c \cot\beta + T\left(h - \frac{D_r}{2}\right)}{a_1 wh \cot\beta - a_1 wh \tan\phi - \frac{1}{2}aa_1 w \tan\phi \cot\beta + \frac{1}{2}a_1^2 w \tan\phi \cot\beta - \frac{1}{2}aa_1 w + \frac{1}{2}a_1^2 w} \quad (32)$$

Substitution of σ into equation (31) provides the value of τ and equation (29) finally yields the predicted failure load of the prism, P. This solution procedure is carried out numerically under varying values of β until a minimum failure load for each specimen is reached. This methodology was considered more sensible than attempting to minimise the failure load with respect to β analytically.

Results from this analysis procedure are shown in Figs 12 and 13, against the existing test results.[1] Correlation calculations again only include those predictions where wedging failure occurred in the tests. Because this is an equilibrium calculation, it is assumed that either *all* the steel yields or only the steel to depth $2{\cdot}4a$ yields.[1]

Comparison between the correlation calculations of Figs 5 and 12 shows that the equilibrium method predicts fairly similar failure loads to those of the simple plane strain translational upper-bound method. Where only steel to a depth of $2{\cdot}4a$ is assumed to have yielded at failure (Fig. 13), accurate correlation is again obtained.

The equilibrium method is clearly simple and fairly accurate when compared with the test results, so it is useful for general wedging analysis of prisms. It suffers from similar limitations to those encountered in the upper-bound methods developed earlier in that it is a purely planar analysis technique. However, out-of-plane effects ought to be checked in practice to ensure that unexpected failures do not occur. In addition, the presence of ducts in practical prisms for anchorage zones cannot be modelled adequately by this method due to the planar nature of the analysis technique. Moreover, the necessity for some measure of the cracking resistance of the prisms exists. These requirements are beyond the scope of this method.

Conclusions

Predictions from the upper-bound plane strain analyses developed here are reasonably good on the whole. It has been found that, although rotation of the outer blocks occurred during testing, the translational mechanism is predicted to occur *before* any rotations, based on zero friction on the base of the specimens. This friction clearly affects the analysis and if it is therefore assumed (from experimental evidence) that the translational mechanism cannot develop in practice, it has been shown that, in general, a curved wedge yield line ought to develop. It is, however, debatable whether there is a necessity for such sophistication in the model. The original plane strain model, including simple translation of the outer blocks only, produced fairly accurate predictions itself, regardless of the neglect of friction on the base.

A particularly simple equilibrium solution was developed for the wedging failure mechanism. It is clear that this method allows quick and simple solutions to the wedging problem for strip-loaded rectangular prisms to be obtained.

It has not, however, been possible to compare results from the above plasticity solutions with those experimental results where failure was predominantly by out-of-plane

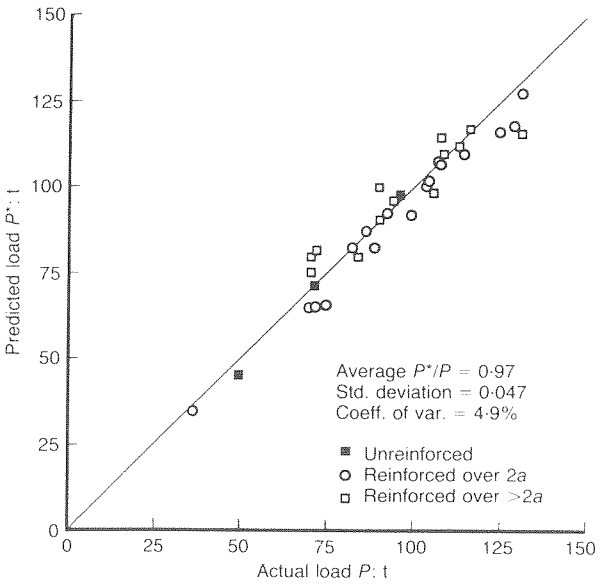

Fig. 12. Comparison between test results and predictions from the equilibrium model, with all steel assumed to have yielded

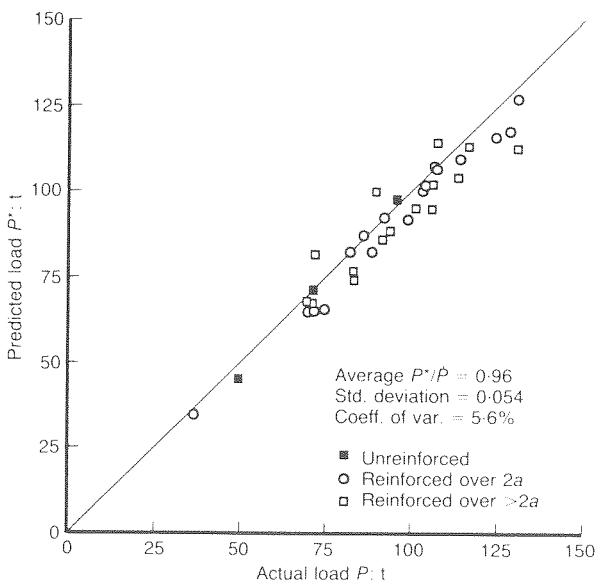

Fig. 13. Comparison between test results and predictions from the equilibrium model, with steel assumed to have yielded to a depth of 2·4a

wedging. In addition, the presence of ducts and prediction of the initial cracking behaviour of the test specimens cannot be modelled by such plasticity methods.

References

1. IBELL T. J. and BURGOYNE C. J. An experimental investigation of the behaviour of anchorage zones, *Mag. Concr. Res.*, 1993, **45**, 281–292.
2. CHEN W. F. and DRUCKER D. C. Bearing capacity of concrete blocks or rock, *J. Engng Mech. Div. Am. Soc. Civ. Engrs*, **95**, No. EM4 Aug 1969, 955–978.
3. NIELSEN M. P. *Limit analysis and concrete plasticity*. Prentice-Hall, USA, 1984.
4. HAWKINS N. M. The bearing strength of concrete for strip loadings, *Mag. Concr. Res.*, 1970, **22**, 87–98.
5. JENSEN B. C. Lines of discontinuity for displacements in the theory of plasticity of plain and reinforced concrete, *Mag. Concr. Res.*, 1975, **27**, 143–150.
6. NIELSEN M. P. *et al. Concrete plasticity: Beam shear — Shear in joints — Punching shear*. Special publication, Danish Society for Structural Science and Engineering, 1978.
7. HOFBECK J. A. *et al.* Shear transfer in reinforced concrete, *J. Am. Concr. Inst.*, 1969, No. 66-13, 119–128.
8. IBELL T. J. Behaviour of anchorage zones for prestressed concrete. PhD dissertation, University of Cambridge, 1992.
9. IBELL T. J. and BURGOYNE C. J. An experimental investigation into the behaviour of prestressed concrete end blocks. Technical Report CUED/D–Struct/TR 135, Cambridge University Engineering Department, May 1991.
10. BRITISH STANDARDS INSTITUTION. *Structural use of concrete*. BSI, London, BS 8110. Part 1: 1985.
11. FENWICK R.C. and LEE S. C. Anchorage zones in prestressed concrete members, Mag. Concr. Res., **38**, 1986, 77–89.

Discussion contributions on this Paper should reach the Editor by 30 September 1994